-RESEARCH PAPER-

International Journal of Mining and Geo-Engineering

IJMGE

IJMGE 57-1 (2023) 41-46

DOI: 10.22059/IJMGE.2022.342045.594969

2D inversion of magnetic and gravity data: a case study on Golgohar mine

Hamid Bizhani [a, *], Pardis Mansour Shoar [b], Meysam Moghadasi [a]

[a] *Faculty of Mining, Petroleum & Geophysics Engineering, Shahrood University of Technology, Shahrood, Iran.*

[b] *Institute of Geophysics University of Tehran, Tehran, Iran.*

Article History:

Received: 24 April 2022.

Revised: 20 July 2022.

Accepted: 22 July 2022.

ABSTRACT

Because of the limitations of manipulating single geophysical data sets to interpret subsurface anomalies for many cases, it is required to combine geophysical data to decrease the ambiguity and non-uniqueness of the interpretation. Integration interpretation of two different geophysical data sets is one of the most common ways to integrate geophysical data and in this paper, we want to utilize the combination of gravity and magnetic data for the Golgohar mine in Iran. This mining case is located in the Sanandaj-Sirjan zone in the province of Kerman. Gravity and magnetic data are interpreted using a MATLAB code written based on the damped weighted minimum length solution for which the model weighting is the product of the multiplying of compactness and depth weighting constraints. At first, the inversion algorithm is applied to the synthetic case to investigate its reliability for practical application on real data. Reconstructed models from the noise-contaminated synthetic data are suggestive of the productivity of the inversion algorithm. Ultimately, the algorithm is applied for the interpretation of the real data and the inversion results of both data sets show a high correlation between the magnetite anomaly position horizontally and vertically. The results represent an anomaly with the depth ranging approximately from 25 to 130 m with the horizontal extension of about 120 m from 280 to 400 m relative to the start of the interesting profile.

Keywords: *Gravity, Inversion, Integration Interpretation, Magnetic, Mining.*

1. Introduction

Gravity method is an efficient technique for mining [1], oil and gas explorations [2, 3], tectonic studies [4], and environmental and geotechnical investigations [5, 6]. Magnetic method is a widespread and reliable tool for different practical applications such as mining cases [7, 8], archeological studies [9, 10], oil and gas explorations [3, 11], and geothermal prospecting [12], and groundwater investigations [13]. However separate gravity or magnetic methods are efficient methods to delineate subsurface targets but it should be mentioned that the integration of geophysical data like gravity and magnetic data can lead to more realistic models for the subsurface structure [10, 14]. Furthermore, in many cases, a single geophysical method results in a poor image from the subsurface targets imposing to use of more than one data set for the anomaly reconstructions [15].

The geophysical data integration is commonly made in three ways: I) joint interpretation [16, 17], II) cooperative inversion [18, 19], and III) joint inversion [20, 21, 22]. In this paper, we want to use the Integration interpretation of gravity and magnetic data for the magnetite mine of Golgohar in Kerman (Iran). Golgohar mine is located in the central part of Sanandaj-Sirjan zone which is stretched from the southwest of central Iran to the northwest of Iran. Because of the large amount of geological activity, it is considered the most unstable geostructural zone in the country. At first, the adopted inversion procedure is introduced which utilizes the compactness and depth weighting functions, then, its reliability is tested on the synthetic data. Ultimately, the inversion algorithm is used to invert both measured gravity and magnetic data to reconstruct the magnetite anomaly position.

2. Methodology

2.1. 2D Forward problem of gravity and magnetic methods

Discretizing subsurface to a lot of prisms composed of four sides (prisms with a rectangle or square cross-section), with infinite length along the geological strike (y direction) and assuming constant susceptibility in each cell, 2-D forward response of the magnetic anomaly can be computed from the following equation [23]:

$$T_i = \sum_{j=1}^{M} \sum_{l=1}^{4} (\hat{f}_x B_x^l + \hat{f}_z B_z^l)_j + e_i , \qquad i = 1, 2, \cdots, N \tag{1}$$

T_i is magnetic anomaly response in the ith observation point, $\hat{f}_x$ and $\hat{f}_z$ are unit components of geomagnetic field and e_i is ith element of the added noise vector to the data, and B_x^l and B_z^l are the x and z components of **B** due to side l which can be calculated using the following formula [23]:

$$B_x = -2C_m(\mathbf{M} \cdot \hat{n})[\hat{s}_x \log\left(\frac{r_{p+1}}{r_p}\right) - \hat{s}_z(\theta_p - \theta_{p+1})]$$

and

$$B_z = -2C_m(\mathbf{M} \cdot \hat{n})[\hat{s}_z \log\left(\frac{r_{p+1}}{r_p}\right) + \hat{s}_x(\theta_p - \theta_{p+1})] \tag{2}$$

r_p, r_{p+1}, θ_p, θ_{p+1} are shown in Fig. 1, **M** is the magnetization vector, $\hat{n}$ is a unit vector perpendicular to each cell, $\hat{s}_x = -\widehat{n_z}$, $\hat{s}_z = -\widehat{n_x}$ and $C_m = \frac{\mu_0}{4\pi} = 10^{-7}$ in SI system units.

* Corresponding author. Tel/Fax: +98-9104864660, *E-mail address:* hamidbizhani.k.a@gmail.com (H. Bizhani).

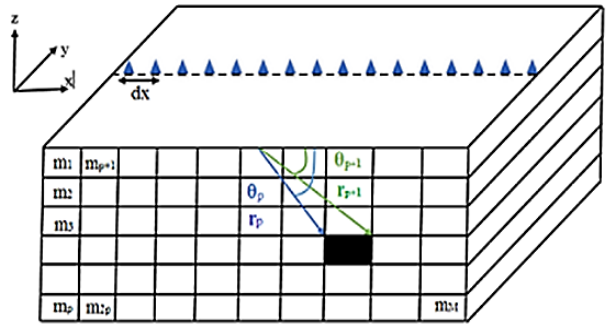

Fig 1. Discretization of the subsurface to a lot of prismatic cells with infinite length along y direction.

Similarly, for the 2-D forward problem of gravity method, considering the subsurface of the interested area is discretized into a lot of prismatic cells infinitely elongated in strike direction (here y direction) and assuming constant density contrast for each cell (Fig. 2), the forward response of the anomaly can be computed by the following formula:

$$g_i = \sum_{j=1}^{M} A_{ij} m_j + e_i \qquad i = 1.2. \ldots . N \tag{3}$$

g_i is ith calculated data, A_{ij} is an element of kernel matrix (forward operator) representing the jth cell effect on ith data, m_j is density contrast of jth cell and e_i is ith element of the added noise vector to the data.

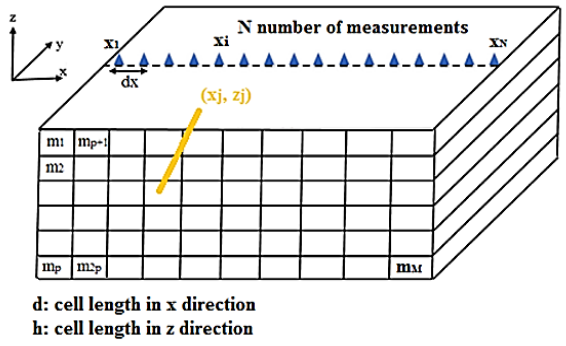

Fig 2. Discretization of the subsurface into the infinitely elongated prismatic cell along strike direction which is here y direction.

A_{ij} elements can be obtained according to the following equation [24]:

$$A_{ij} = 2\gamma\left[\left(x_i - x_j + \frac{d}{2}\right) log\left({}^{r_2 r_3}/_{r_1 r_4}\right) + d\, log\left({}^{r_4}/_{r_3}\right) - \left(z_j + \frac{h}{2}\right)(\theta_4 - \theta_2) + \left(z_j - \frac{h}{2}\right)(\theta_3 - \theta_1)\right] \tag{4}$$

As mentioned in (Fig.2), d and h are cell lengths in the x and z direction, respectively and γ is the gravitational constant, and r and θ may be calculated as [24]:

$$r_1^2 = (z_j - \frac{h}{2})^2 + (x_i - x_j + \frac{d}{2})^2 \qquad \theta_1 = \arctan\,(x_i - x_j + \frac{d}{2})/(z_j - \frac{h}{2})$$
$$r_2^2 = (z_j + \frac{h}{2})^2 + (x_i - x_j + \frac{d}{2})^2 \qquad \theta_2 = \arctan\,(x_i - x_j + \frac{d}{2})/(z_j + \frac{h}{2})$$
$$r_3^2 = (z_j - \frac{h}{2})^2 + (x_i - x_j - \frac{d}{2})^2 \qquad \theta_3 = \arctan\,(x_i - x_j - \frac{d}{2})/(z_j - \frac{h}{2})$$
$$r_4^2 = (z_j + \frac{h}{2})^2 + (x_i - x_j - \frac{d}{2})^2 \qquad \theta_4 = \arctan\,(x_i - x_j - \frac{d}{2})/(z_j + \frac{h}{2})$$

For both methods, the forward problem can be written as:

$$\mathbf{d}=\mathbf{Am} \tag{5}$$

A is the forward operator, **m** is the model vector and **d** is the vector of data.

2.2. Inversion

Potential field data inversion is confronted with two main ambiguities: I) theoretical ambiguity due to the Gauss' theorem by which many equivalent sources can produce the same known field at the surface, and II) algebraic ambiguity because the number of model parameters (unknowns) is more than data points. In addition to the mentioned ambiguities, data always are contaminated by some noise and this noise can propagate large errors into the reconstruction process of the subsurface model. So, the inverse problem is non-unique and unstable, and introducing a priori information and constraints are required in order to obtain a desirable inversion model from measured data. During the last decades, different algorithms have been proposed by geophysicists for potential field data inversion [24, 25, 26, 27, 28, 29, 30, 31]. In this paper, a damped weighted minimum length solution is utilized for both methods. Minimizing the following objective function leads to an inversion solution of the linear system of equations (5), [32]:

$$\min \rightarrow \|\boldsymbol{W}_d(\boldsymbol{Am}-\boldsymbol{d})\|_2^2 + \alpha\|\boldsymbol{W}_m(\boldsymbol{m}-\boldsymbol{m}_r)\|_2^2 \tag{6}$$

Where $\boldsymbol{m}_r$ is the reference model assumed to be zero, α is the regularization parameter and $\boldsymbol{W}_d$ and $\boldsymbol{W}_m$ are data and model weighting matrices, respectively. We assume that $\boldsymbol{W}_d$ to be an identity matrix. Solving equation (6) can lead to the following weighted damped minimum length solution [33]:

$$\boldsymbol{m} = \boldsymbol{m}_r + (\boldsymbol{W}_m^{-1}\boldsymbol{A}^T)(\boldsymbol{A}\boldsymbol{W}_m^{-1}\boldsymbol{A}^T + \alpha\boldsymbol{W}_d)^{-1}(\boldsymbol{d}-\boldsymbol{A}\boldsymbol{m}_r) \tag{7}$$

$\boldsymbol{W}_m$ is a model weighting matrix produced by the multiplication of compactness and depth weighting functions. Compactness constraint which is proposed by Last and Kubic as [24]:

$$\boldsymbol{W}_c = \frac{1}{(\boldsymbol{m}+\varepsilon)^2} \tag{8}$$

$\boldsymbol{m}$ is the model parameter vector and ε is a very small value preventing the denominator to be zero. The depth weighting matrix was introduced by Li and Oldenburg (1996) [34], as the following formula:

$$\boldsymbol{W}_z = \frac{1}{(\boldsymbol{Z})^{(\beta/2)}} \tag{9}$$

$\boldsymbol{Z}$ is the vector of cell center coordinates and β is the depth weighting exponent. Li and Oldenburg Suggested β to be 3 and 2 for magnetic and gravity methods, respectively (1996 and 1998) [34, 27].

Cella and Fedi (2012) [30], introduced an objective technique for the estimation of the depth weighting exponent. They attributed the structural index value to the exponent of depth weighting which can be estimated by methods such as Euler deconvolution or DEXP [35]. Here, for all synthetic and real cases, β=2 seems to be the best choice. Fig. 3 represents the flowchart of the inversion algorithm which is going to be manipulated here. Regularization parameters can be estimated using standard methods such as L-curve or generalized cross validation (GCV) but here it is estimated according to the maximum (Max) value of the kernel matrix for both gravity and magnetic cases and the suggested value is α=0.1×Max(A)[36]. This interesting point was obtained through its testing for different cases and it can be manipulated for noisy synthetic data with noise levels up to 5%. For the higher level of noise, a larger value is required. In addition, α=0.1×Max(A) value works very well for real data sets as will be shown in the real data section. To end this, we should mention that we don't want to assert introduce a new method to estimate the regularization parameter, rather we described exactly how we estimated α. The acceptance/declination of the suggested value as a method for regularization parameter estimation demands a comprehensive investigation including mathematical justification which is beyond the scope of this paper.

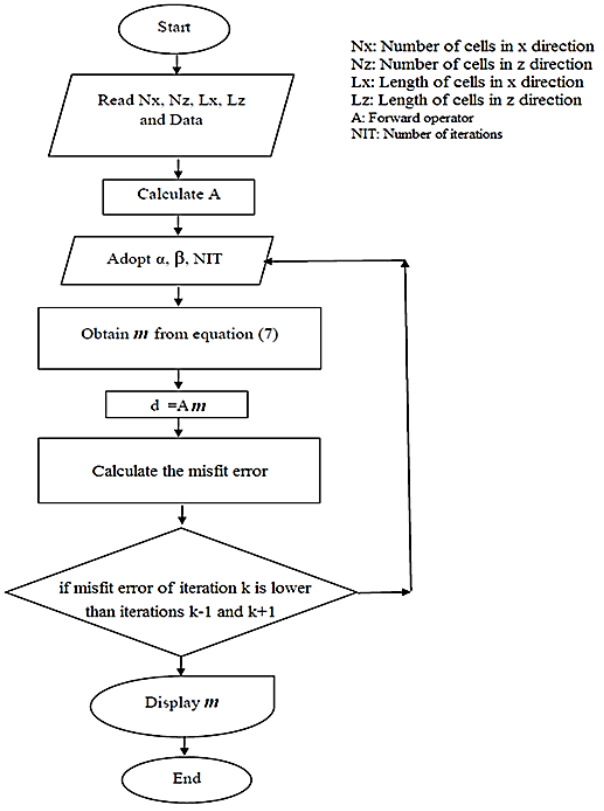

Fig 3. Flowchart of inversion algorithm for gravity and magnetic data.

2.3. Synthetic modeling

Before applying the inversion algorithm to the field data set, we should test its productivity through its implementation on synthetic data to see if the algorithm is enough promising for practical applications. A synthetic model composed of two compact bodies is considered (Fig. 4) and the characteristics of the anomalies are specified in Tab. 1. Synthetic data for the assumed models were obtained and 5 % random noise was added to the data. Inverted gravity and magnetic models derived from the inversion algorithm are represented in Fig. 5. The depth ranges and density values of both anomalies are well recovered by gravity data inversion and only the horizontal extension of the deeper block is less than the true model. For the magnetic method, the depth and horizontal ranges of both blocks are in very good agreement with the blocks of the true model. Furthermore, susceptibility of the deeper block is also well retrieved but the shallower block susceptibility has some differences with true value. In conclusion, it can be said that the performance of the adopted inversion algorithm is satisfactory due to the presence of 5% random noise on the data and give enough reliability to be manipulated for the field data set. Inversion parameters chosen for the inverse process of both gravity and magnetic data can be found in Tab. 2. From the table it can be understood that the regularization parameters of both methods are similarly adopted according to the maximum value of the forward operator (Max(A)) as one-tenth of this value. Depth weighting exponents for both methods were 2. In addition, it was demonstrated that the number of iterations (NIT) of 3 leads to satisfactory inversion models and data misfits (Fig. 6) for both methods. NIT is chosen so that the misfit RMS error of computed data with observed data for iteration k is lower than iterations k-1 and k+1. RMS error is calculated from the following equation:

$$\text{RMS error}=\sqrt{\frac{\sum_{i=1}^{N}(d_{obs}-d_{pre})^2}{N}} \quad (10)$$

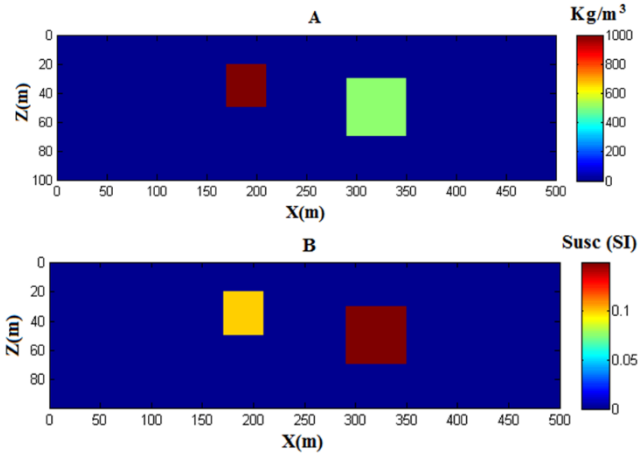

Fig 4. True models of gravity (A) and magnetic (B) methods are composed of two blocks.

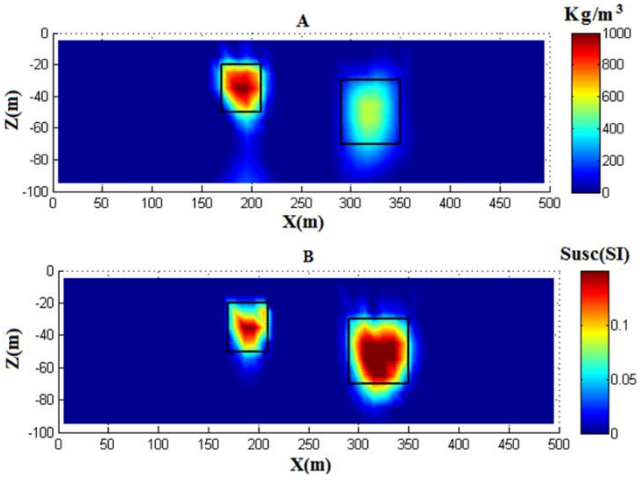

Fig 5. Inversion models derived from synthetic data contaminated by 5% random noise for gravity (A) and magnetic (B) methods.

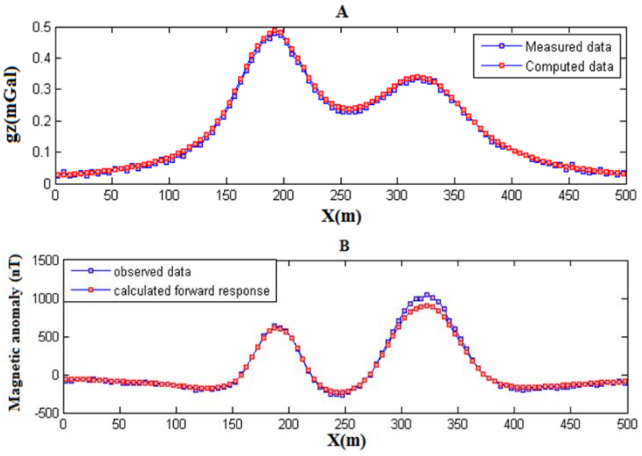

Fig 6. Observed data and computed data from inversion models of gravity (A) and magnetic (B) methods.

Table 1. Characteristics of the anomalies considered for the synthetic modeling.

Block	Horizontal position (m)	Vertical position (m)	Susceptibility contrast (SI)	Density contrast (g/cm³)
Shallow	170-210	20-50	0.1	1
Deep	290-350	30-70	0.15	0.5

Table 2. Inversion parameters were adopted for gravity and magnetic synthetic data sets.

Method	α	β	NIT	Misfit error
Gravity	0.1×Max(A)	2	3	4.87
Magnetic	0.1×Max(A)	2	3	4.35

Where d_{obs} and d_{pre} are observed and predicted data, respectively, and N is the number of data points.

3. Real data

3.1. The situation and general geology of Golgohar mineral zone

From the geological point of view, Golgohar mineral zone is situated in the southern part of Sanandaj-Sirjan zone (Fig. 7). The general trend of this zone is northwest-southeast. Sanandaj-Sirjan zone is a beam from the southwest of central Iran to the northeast of Zagros main thrust. This zone is approximately 1500 km long and extended from the west of Lake Urmia to the east of Bandar Abbas (near Hajiabad). Due to the existence of a large number of metamorphism phenomena, magmatism, and successive tectonic processes in this zone, it is taken into consideration as the most unstable geostructural zone in Iran. This region has complex structures and due to the different occurred metamorphisms in this zone, it is very difficult to find the ages and relations of the geological units. Golgohar mineral zone is generally covered by alluviums and rare heights, including Paleozoic metamorphic rocks in the south and southwest and Mesozoic and Cenozoic sedimentary rocks in the east of the zone. Paleozoic rocks, including Golgohar complex, form the oldest metamorphic assemblage in this zone. In Golgohar zone, only a part of the rocks of Golgohar metamorphic complex is exposed. The lower part of this complex consists of alternating gneisses, mica schists, amphibolites, and quartz schists, on which alternating dolomitic marbles, mica schist, greenschist, and graphitic schist are situated without unconformity. This complex is ended in a dolomitic or calcite marble unit, known as Kore Sefid in the whole Sanandaj-Sirjan zone.

3.2. Inversion models and Interpretation

Fig. 9 shows the residual anomalies of the collected gravity and magnetic data with the considered profile (a-b) for the inversion procedure. The number of data for each profile is 60 and the length of the profile is 590 m. The subsurface is divided into 60 by 20 square cells along x and z directions, respectively, with a side length of 10 m. According to this discretization, the data points are in the middle of each cell 5, 15, 25, ..., 595 m. Gravity and magnetic inversion sections are shown in Fig. 10, while Fig. 11 represents the measured data and computed data from inversion results for both methods. The selected inversion parameters and misfit errors can be found in Tab. 3. From the inversion results, the gravity method approximately produces an anomaly in the depth range of 25 to 130 m with horizontal extension from 300 to 400 m. Magnetic data inversion approximately reconstructs an anomaly with a depth range from 30 to 130 m and horizontal position from 280 to 400 m. However, it should be mentioned that, despite these horizontal and vertical extension agreements, the anomaly boundaries and therefore its shapes in two inversion sections are not in perfect correspondence. In conclusion, both retrieved sections demonstrate a high correlation between the horizontal and vertical position of the magnetite anomaly. High recovered susceptibility from the magnetic data inversion is consistent with the magnetite mine mass.

Tab. 3 tells us that the regularization parameter equal to 0.1×Max(A) for both methods leads to the desired solutions. In addition, the depth weighting exponent and number of iterations of 2 and 3, respectively, show to be enough appropriate for getting the inversion sections. Low misfit error values and the results displayed in Fig. 10 are expressive of perfect computed data fit with the measured data quantitatively and qualitatively, respectively.

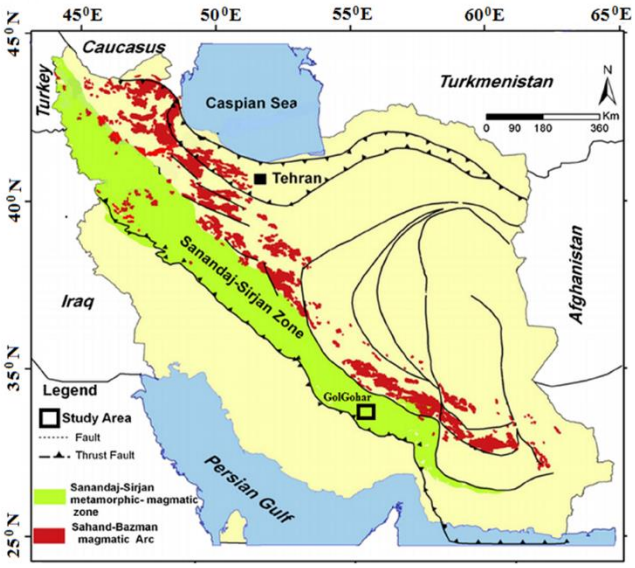

Fig 7. Sanandaj-Sirjan zone and the location of the Golgohar mine in the Iran geography map (Sahandi et al., 2005) [37].

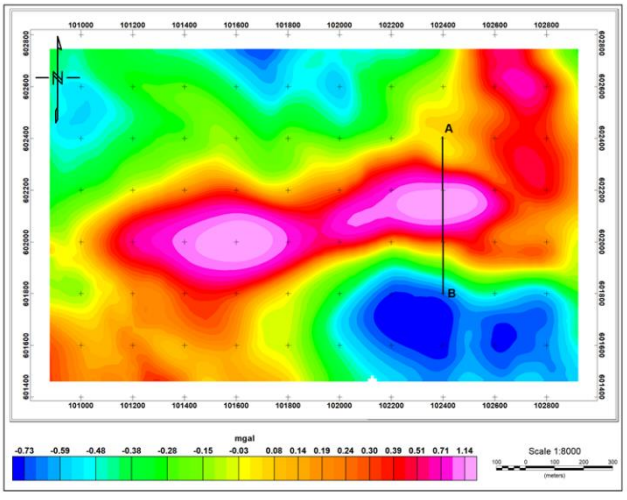

(A)

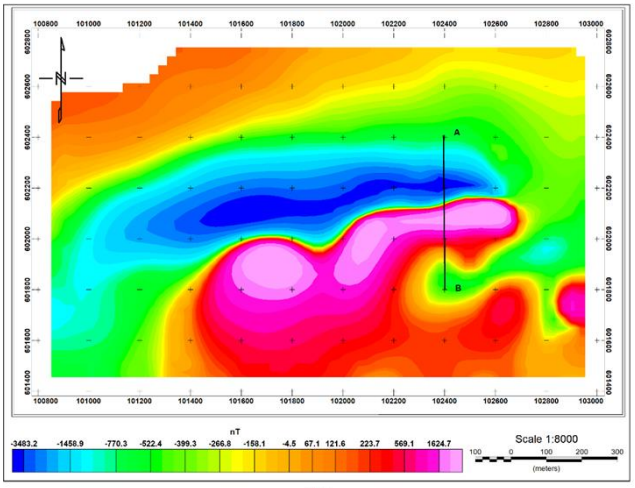

(B)

Fig 9. Residual (A) gravity and (B) magnetic anomaly maps. Interested profiles (a-b) of gravity and magnetic data for inversion are shown on the corresponding maps.

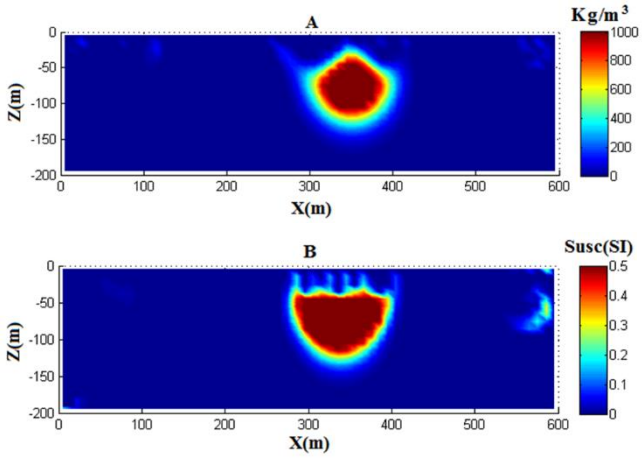

Fig 10. Inversion models are derived from the gravity (A) and magnetic (B) real data sets.

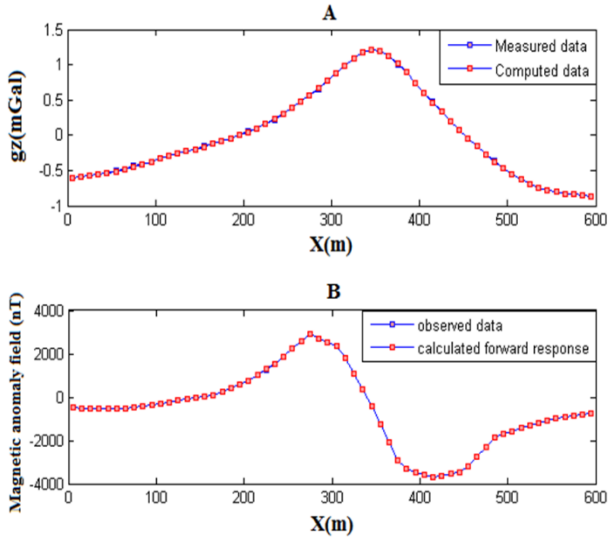

Fig 11. Measured data and computed data from inversion models of gravity (A) and magnetic (B) methods.

Table 3. Inversion parameters were adopted for gravity and magnetic real data sets.

Method	α	β	NIT	Misfit error
Gravity	0.1×Max(A)	2	3	1.14
Magnetic	0.1×Max(A)	2	3	1.73

4. Conclusion

Geophysical data integration through enhanced known information leads to a more reliable interpretation of the subsurface targets. In this paper, Integration interpretation of gravity and magnetic data sets are exploited for the magnetite mining case of Golgohar located in the Sanandaj-Sirjan zone in Kerman (Iran), and individual inversions were obtained using the damped weighted minimum length solution algorithm taking the advantage of a model weighting matrix derived from the multiplication of the compactness and depth weighting functions. At first, the algorithm was applied to the noise-contaminated synthetic data sets of gravity and magnetic. Since the inversion results were enough promising, we decide to use the inversion algorithm to interpret the real case. Derived inversion sections for both gravity and magnetic data sets were in high correlation suggesting the magnetite anomaly in the depth range from 25 to 130 m with horizontal position from 280 to 400 m.

Acknowledgment

The authors thank Dr. Ramin Varfinezhad for providing us with his inversion codes as well as his assistance during the process of writing this paper.

REFERENCES

[1] Martinez, C., Li, Y., Krahenbuhl, R., & Braga, M. A. (2013). 3D inversion of airborne gravity gradiometry data in mineral exploration: A case study in the Quadrilátero Ferrífero, Brazil. Geophysics, 78(1), B1-B11

[2] Nettleton, L. L. (1976). Gravity and Magnetics in Oil Prospecting. McGraw-Hill Companies.

[3] Al-Farhan, M., Oskooi, B., Ardestani, V. E., Abedi, M., & Al-Khalidy, A. (2019). Magnetic and gravity signatures of the Kifl oil field in Iraq. Journal of Petroleum Science and Engineering, 183, 106397.

[4] Paterson, N. R., & Reeves, C. V. (1985). Applications of gravity and magnetic surveys: The state-of-the-art in 1985. Geophysics, 50(12), 2558-2594.

[5] Hinze, W. J. (1990). The role of gravity and magnetic methods in engineering and environmental studies. In Geotechnical an Environmental Geophysics: Volume I: Review and Tutorial (pp. 75-126). Society of Exploration Geophysicists.

[6] Ward, S. H. (Ed.). (1990). Geotechnical and Environmental Geophysics: Volume I, Review and Tutorial: Volume I: Review and Tutorial. Society of Exploration Geophysicists.

[7] Sharma, P. V. (1987). Magnetic method applied to mineral exploration. Ore geology reviews, 2(4), 323-357.

[8] Cheng, Z. L., Zuo, Q. H., & Wang, J. F. (2013). Magnetic prospecting on magnet mining exploration area of Laos bokeo province. Progress in Geophysics, 3.

[9] Eppelbaum, L. V. (2011). Study of magnetic anomalies over archaeological targets in urban environments. Physics and Chemistry of the Earth, Parts A/B/C, 36(16), 1318-1330.

[10] Varfinezhad, R., Oskooi, B., & Fedi, M. (2020). Joint Inversion of DC Resistivity and Magnetic Data, Constrained by Cross Gradients, Compactness and Depth Weighting. Pure and Applied Geophysics, 1-19.

[11] Eventov, L. (1997). Applications of magnetic methods in oil and gas exploration. The Leading Edge, 16(5), 489-492.

[12] Zaher, M. A., Saibi, H., Mansour, K., Khalil, A., & Soliman, M. (2018). Geothermal exploration using airborne gravity and magnetic data at Siwa Oasis, Western Desert, Egypt. Renewable and Sustainable Energy Reviews, 82, 3824-3832.

[13] Oni, A. G., Eniola, P. J., Olorunfemi, M. O., Okunubi, M. O., & Osotuyi, G. A. (2020). The magnetic method as a tool in groundwater investigation in a basement complex terrain: Modomo Southwest Nigeria as a case study. Applied Water Science, 10(8), 1-18.

[14] Fregoso, E., & Gallardo, L. A. (2009). Cross gradients joint 3D inversion with applications to gravity and magnetic data. Geophysics, 74(4), 31–42.

[15] Joulidehsar, F., Moradzadeh, A., & Doulati Ardejani, F. (2018). An improved 3D joint inversion method of potential field data using cross-gradient constraint and LSQR method. Pure and Applied Geophysics, 175, 4389–4409

[16] Orlando, L. (2005). Joint interpretation of geophysical data for

archaeology. A case study. Subsurface Sensing Technologies and Applications, 6(2), 235–250.

[17] Ogaya, X., Alcalde, J., Marza´n, I., Ledo, J., Queralt, P., Marcuello, A., et al. (2016). Joint interpretation of magnetotellurics, seismic, and well-log data in Hontomı´n (Spain). Solid Earth, 7, 1–15.

[18] Singh, A., Mishra, P. K., & Sharma, S. P. (2019). 2D cooperative inversion of direct current resistivity and gravity data: A case study of uranium-bearing target rock. Geophysical Prospecting, 67(3), 696-708

[19] Moradi, M., Oskooi, B., Pushkarev, P., Smirnov, M., & Oghaz, H. E. (2019). Cooperative inversion of magnetotelluric and seismic data on Shurab diapirs in Central Iran. Environmental Earth Sciences, 78(11), 1-14.

[20] Gallardo, L. A., & Meju, M. A. (2011). Structure coupled multiphysics imaging in geophysical sciences. Reviews of Geophysics, 49, RG1003.

[21] Varfinezhad, R., Hafizi, M. K., & Hashemi, H. (2015). Application of different inverse methods for combination of vS and vGPR data to estimate porosity and water saturation. Journal of the Earth and Space Physics, 41(4), 89-94.

[22] Wang, K. P., Tan, H. D., & Wang, T. (2017). 2D joint inversion of CSAMT and magnetic data based on cross-gradient theory. Applied Geophysics, 14(2), 279–290.

[23] Blakely, R. J. (1996). Potential Theory In Gravity And Magnetic Applications. Cambridge university press.

[24] Last, B. J., & Kubik, K. (1983). Compact gravity inversion. Geophysics, 48(6), 713-721.

[25] Guillen, A., & Menichetti, V. (1984). Gravity and magnetic inversion with minimization of a specific functional. Geophysics, 49(8), 1354-1360.

[26] Barbosa, V. C. F., & Silva, J. B. (1994). Generalized compact gravity inversion. Geophysics, 59(1), 57-68.

[27] Li, Y., & Oldenburg, D. W. (1998). 3-D inversion of gravity data. Geophysics, 63(1), 109-119.

[28] Ansari, A., Pasyar, A., Ghorbani, A. (2022). Solving 2-D gravity inversion problems using a PDE model in geophysics exploration. International Journal of Mining and Geo-Engineering, doi: 10.22059/ijmge.2021.317502.594888

[29] Boulanger, O., & Chouteau, M. (2001). Constraints in 3D gravity inversion. Geophysical prospecting, 49(2), 265-280.

[30] Cella, F., & Fedi, M. (2012). Inversion of potential field data using the structural index as weighting function rate decay. Geophysical Prospecting, 60(2), 313-336.

[31] Paoletti, V., Ialongo, S., Florio, G., Fedi, M., & Cella, F. (2013). Self-constrained inversion of potential fields. Geophysical Journal International, 195(2), 854-869.

[32] Tikhonov, A. N., & Arsenin, V. Y. (1977). Solutions of ill-posed problems. New York, 1-30.

[33] Menke, W. (2012). Geophysical data analysis: discrete inverse theory, MATLAB edn. New York: Academic.

[34] Li, Y., & Oldenburg, D. W. (1996). 3-D inversion of magnetic data. Geophysics, 61(2), 394-408.

[35] Fedi, M. (2007). DEXP: A fast method to determine the depth and the structural index of potential fields sources. Geophysics, 72(1), I1-I11.

[36] R. Varfinezhad and V.E. Ardestani (2021). Kernel-based regularisation parameter and source-dependent depth weighting in gravity data inversion. Bulletin of Geophysics and Oceanography, pp. 249-266.

[37] Sahandi MR, Delavar ST, Sadeghi M, Jafari A, Moosavi A (2005). Geological map of Iran (1:1,000,000) Geological survey of Iran.